

3D discrete simulations of fracture in concrete specimens

S. Saito & T. Higai

University of Yamanashi, Kofu, Japan

ABSTRACT: Rigid-body-spring networks with random geometry provided by a Voronoi discretization are used to investigate the fracture behavior of cement based composites. The material mesostructure is three-dimensionally modeled using a three component model: mortar matrix, aggregate inclusions, and matrix-inclusion interfaces. Model abilities to predict stress-strain responses and crack patterns are demonstrated through analyses of compact tension and uniaxial compression tests. Macro-failure of concrete is simulated by only local tension and shear fracture of particle interfacial springs at meso-scale.

1 INTRODUCTION

Fracture of heterogeneous and quasi-brittle materials like concrete can be characterized by the initiation and propagation of microcracking, followed by the localization of such damage into relatively narrow zones. Discrete crack models have been used to simulate the fracture processes in concrete materials since the localization of fracture causes a strong discontinuity within the material domain.

Random particle models and lattice models have been used to study various fracture behaviors of cement based composites (e.g. Bazant et al. 1990; Schlangen & van Mier 1992; Schlangen 1995). Concrete material is modeled by a network of simple spring-like elements which are interconnecting regularly or randomly distributed particles (i.e. nodal sites). The link between particles is assumed to transmit only axial forces and the particle rotation and transmission of shear are neglected in the early random particle models (Bazant et al. 1990). Lattice models consist of beam-springs which resist not only axial forces but also bending, so that it has advantages in modeling apparent shear transfer mechanisms (Schlangen & van Mier 1992).

Cement based composites can be modeled by a multi-phase material (e.g. matrix, aggregate, and matrix-aggregate interface). In lattice-type models, springs are assigned different properties according to the phase being represented. These models have applied to analyze brittle fracture of cement composites dominated by tensile cracking and exhibited good agreement with experimental observations. There have, however, been difficulties in predicting compressive strength by using these simple models

since concrete under compressive stresses exhibits rather complicated behavior. Cusatis et al. (2003) have recently found that the following issues should be considered in the lattice-type models to accurately predict fracture behavior of cement composites in compression: (1) three-dimensional modeling is required and constitutive models for the lattice struts need to include inelastic behavior; (2) the lattice struts transfer both axial forces (i.e. tension and compression) and shear forces.

Simulations by these models have so far been mostly two-dimensional, rather than three-dimensional. The fracture criteria of beam-springs are assumed to be sequential elastic-brittle in order to consider three-dimensional effects, and so the link may be gradually removed if the failure criterion is met at one of the beams. This is computationally efficient, but still provides rather brittle behavior.

In the original lattice model, shear transmission may also be achieved due to bending in treating the lattice struts as beams, but the bending is not characteristic of the physical nature in the microstructure.

Rigid-body-spring networks, which have similar features, are being used to analyze fracture in heterogeneous materials (Liu et al. 1995; Bolander & Saito 1998). The material is modeled as an assemblage of rigid particles interconnected by springs (Kawai 1978). The network has advantages in introducing random geometry to reduce mesh bias on fracture direction and in modeling shear transfer using the interfacial transverse springs. Realistic predictions of crack patterns may be obtained, but the quantitative stress-strain responses do not exhibit reasonable agreement with the actual behavior since these models are mostly two-dimensional.

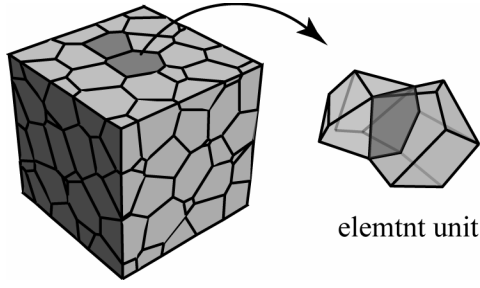


Figure 1. Domain discretization using Voronoi diagrams and a two-continuous particle assembly.

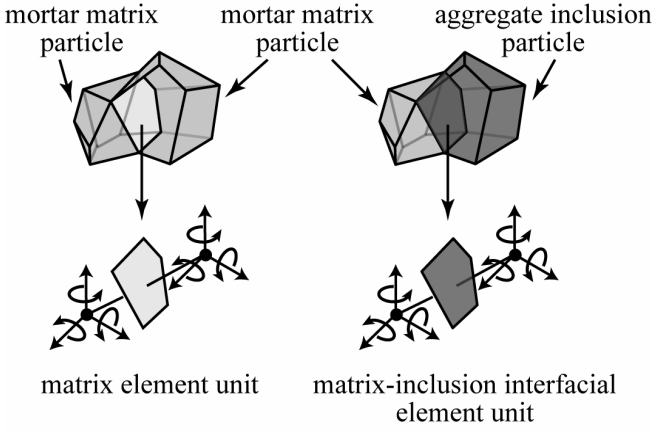


Figure 2. Element unit for different material components.

In this paper, preliminary results are given for tensile and compressive tests of concrete specimens, where fracture simulations are conducted with three-dimensional rigid-body-spring networks.

2 NUMERICAL MODELS

2.1 Model construction

Discrete crack approaches are well suited to problems in which material discontinuities are dominant. Most of these approaches, however, exhibit mesh bias on crack propagation and/or require sophisticated programming to achieve robustness in three-dimensional implementations. As the simplicity of rigid-body-spring networks provides considerable freedom in mesh layout, a random geometry using Voronoi diagrams is introduced to minimize such mesh bias on crack direction (Figure 1). The material domain is discretized using the Voronoi diagram based on an arbitrary (e.g. semi-random) set of points, which are defined as computational nodes. By strategically introducing interior and auxiliary points, domains with arbitrary boundaries and/or inclusions can be discretized in both two- and three-dimensional (Bolander & Saito 1998; Bolander & Berton 2004).

To simulate the meso-structural fracture of cement composites, concrete is represented using a three component model: matrix, aggregate inclusions, and matrix-inclusion interfacial zones. Al-

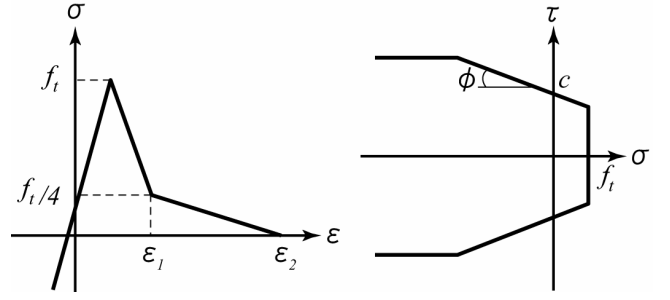


Figure 3. Constitutive model for: a) normal springs and b) tangential springs.

though the ultimate goal is the full modeling of heterogeneity considering various size and distribution of aggregate inclusions based on the actual mix proportion, the computational efforts for such complicated problems in three-dimension become quite large. The heterogeneity in this preliminary work is, thus, modeled by the following discretization process: (1) domain is regularly discretized as matrix using the Voronoi diagram; (2) some of the particle elements are randomly chosen as aggregate inclusions until achieving the appropriate volume. This simple approach allows conducting a parametric study with minimal computational efforts

2.2 Rigid-body-spring network

Each rigid particle has three translational and three rotational degrees of freedom at the interior point. A two-contiguous-particle assembly forms an element unit, as shown in Figure 2. The interface between the particles consists of a zero-size spring set: one normal and two tangential to the facet, and three rotational springs. The interfacial springs, whose initial properties can be set to approximate the elastic properties of the continuum, act at the centroid of the Voronoi facet. The network exhibits elastically uniform during uniform straining by using geometrical properties of the Voronoi diagram, and by setting the appropriate stiffness (Bolander & Saito 1998; Bolander & Berton 2004). For the translational springs:

$$k_x = k_y = k_z = E \frac{A}{h} \quad (1)$$

and for the rotational springs:

$$k_{\alpha_x} = E \frac{J}{h}, \quad k_{\alpha_y} = E \frac{I_1}{h}, \quad k_{\alpha_z} = E \frac{I_2}{h} \quad (2)$$

where E is the elastic modulus; A is the facet area; h is the element length (i.e. the distance between the nodes); I is the principal moment of inertia of area; and J is the polar moment of inertia.

2.3 Fracture criteria

The response of the rigid-body-spring network provides understanding of the interaction between parti-

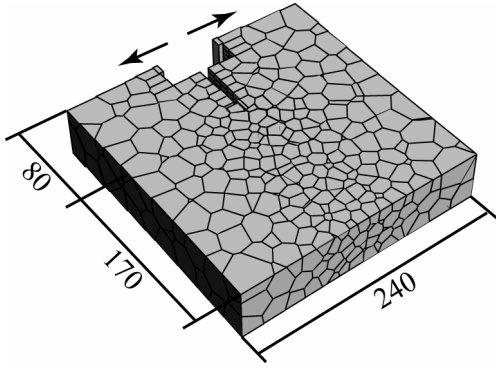


Figure 4. Numerical model of compact tension test specimen.

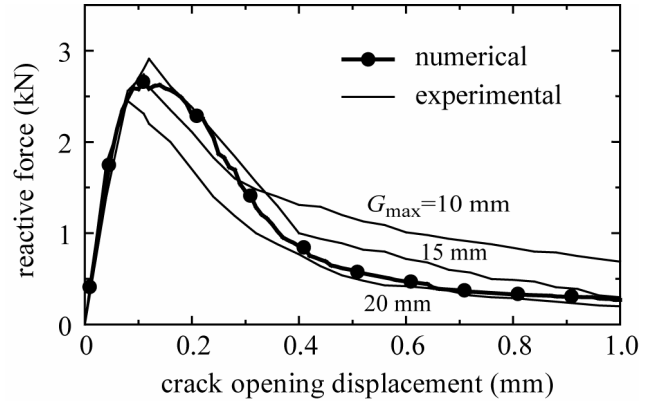


Figure 5. Reactive force-crack opening displacement response.

cles rather than the internal behavior of each particle based on continuum mechanics. The model is therefore suited towards problems where material discontinuities are dominant.

At particle boundaries, normal springs are defined to represent tensile and compressive properties according to the component type. Tensile fracture of the matrix and matrix-inclusion interface is treated by a bilinear function of the spring strain, as shown in Figure 3a. The tensile strength f_t and fracture energy G_f (which defines the strains ε_1 and ε_2) at the weak matrix-inclusion interface is simply set to half of those at the matrix in this work, since the properties of matrix-inclusion interfaces are not well clarified. Note that the compressive fracture of normal springs is not defined in this meso-scale modeling, so that the springs in compression keep their elasticity.

Tangential springs represent the shear transfer mechanism, where the shear strength is assumed to obey a Mohr-Coulomb type of criterion with a tension cap (Figure 3b). The parameters as shown in the figure can be computed from the strength of components, and so the values at the matrix-inclusion interface are also set to half of those at the matrix.

3 COMPACT TENSION TEST SIMULATION

3.1 Analysis model

A concrete compact tension specimen tested by Otsuka & Katsube (1994) is analyzed. Figure 4 shows a numerical model of the test specimen whose dimensions are 240 x 250 x 50 mm. To reduce computational expense, the ligament region is finely discretized and modeled as a three-phase composite. Aggregate elements comprise 30 % of the total volume of particle elements in the ligament region. Physical phenomena observed on a smaller scale should be, therefore, treated at the level of the constitutive models. The used values of the component tensile strength and elastic modulus are: $f_m = 3.5$

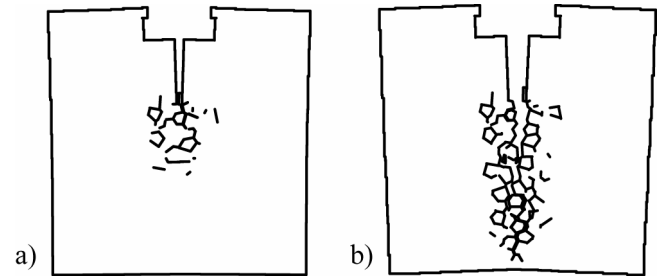


Figure 6. Crack patterns: a) just after the peak load and b) at the final stage of loading.

MPa, $f_{ti} = 1.75$ MPa, $E_m = 20$ GPa, and $E_a = 60$ GPa, where the subscripts a, m, and i denote aggregate, mortar matrix, and interface, respectively. The elastic modulus used for the interface, E_i , is a mean value of E_m and E_a . The fracture energy for the interface, G_{fi} is assumed to be ten percent of that of the matrix, $G_{fm} = 100$ N/m.

3.2 Simulation results

Figure 5 shows the reactive force vs. crack opening displacement response obtained from the simulation. The test results from three specimens with different maximum aggregate size ($G_{max} = 10$ mm, 15 mm, and 20 mm) are also shown for comparison. The mean size of particle elements (i.e. aggregate size in the analysis) is about 12 mm at the ligament region. The numerical result agrees well with the test results. Figure 6 shows the numerical crack patterns just after the peak load and at the final stage of loading. Microcracks initiated from the matrix-aggregate interface can be seen along the main crack path. Three-dimensional analysis with simple modeling of cement composites will provide reasonable predictions for tension problems.

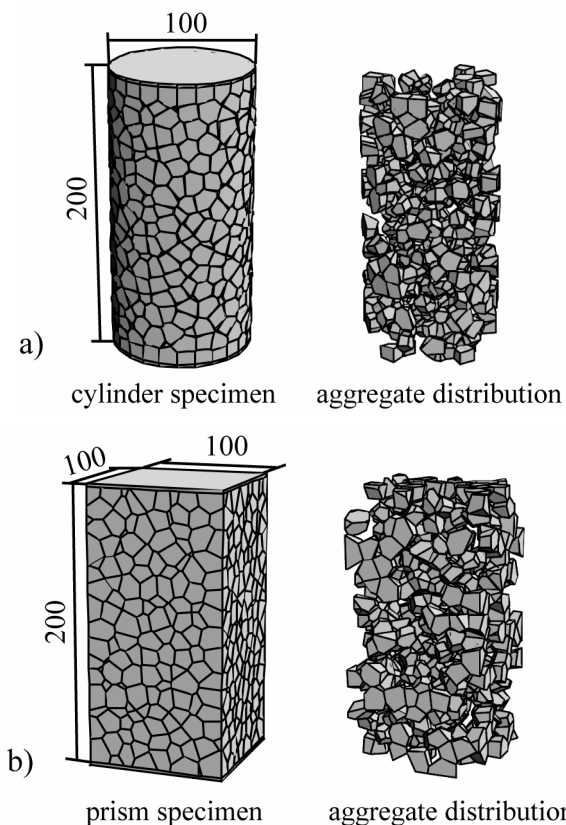


Figure 7. Typical Voronoi mesh and assumed aggregate distribution for: a) cylinder specimen and b) prism specimen.

4 UNIAXIAL COMPRESSION TEST SIMULATION

4.1 Analysis model

Concrete cylinder and prism specimens subjected to uniaxial compression are analyzed. Figure 7 shows the cylinder with a diameter of 100 mm and a height of 200 mm, and prism with a cross section of $100 \times 100 \text{ mm}^2$ and a height of 200 mm. To perform meso-scale analyses, nearly 30% of the total volume of Voronoi particle elements is randomly chosen as aggregate elements, as shown in Figure 7. The same material properties used in the previous section are assumed here.

To confirm the model validation, three specimens with different particle discretization are analyzed for the cylinder and prism, respectively. Figure 8 shows the stress-strain responses obtained from the uniaxial compression test simulation of the cylinders and prisms. The numerical results ideally exhibit no scatter although their mesh design is different. The curves are similar to a general experimental result observed on the behavior of normal strength concrete subjected to uniaxial compression. The rigid-body-spring network with random geometry provides reasonable predictions even if the material properties are rather simply modeled in order to reduce computational expense in three-dimensional analyses.

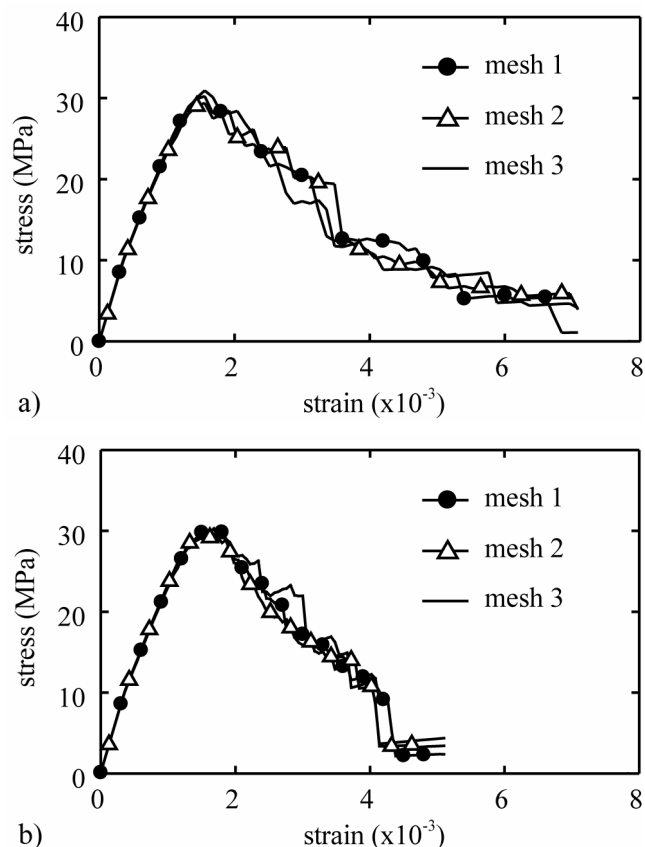


Figure 8. Compressive stress-strain responses for: a) cylinder specimens and b) prism specimens.

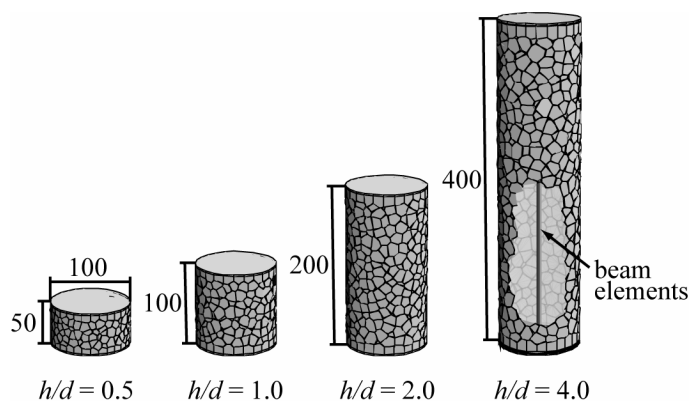


Figure 9. Numerical models for cylinder specimens with different slenderness ratio h/d .

Uniaxial compression tests of concrete cylinders and prisms with various slenderness ratios ($h/d = 0.5, 1.0, 2.0, \text{ and } 4.0$, where h is the specimen height, and the diameter $d = 100 \text{ mm}$) are analyzed in this article. Figure 9 shows the numerical models for cylinder specimens. Fracture localization along the specimen height is investigated by using local strain distribution which is obtained from beam elements placed inside the specimen, as shown in Figure 8. The effects of friction between the specimen ends and the loading plates are considered by assuming two conditions in shear springs: (1) low friction modeled by eliminating shear stiffnesses between the plate and the specimen; and (2) high friction produced by imposing the frictional force $F = \mu R$, where R is the reaction, and the coefficient of friction $\mu = 0.2$ (Cusatis et al. 2003).

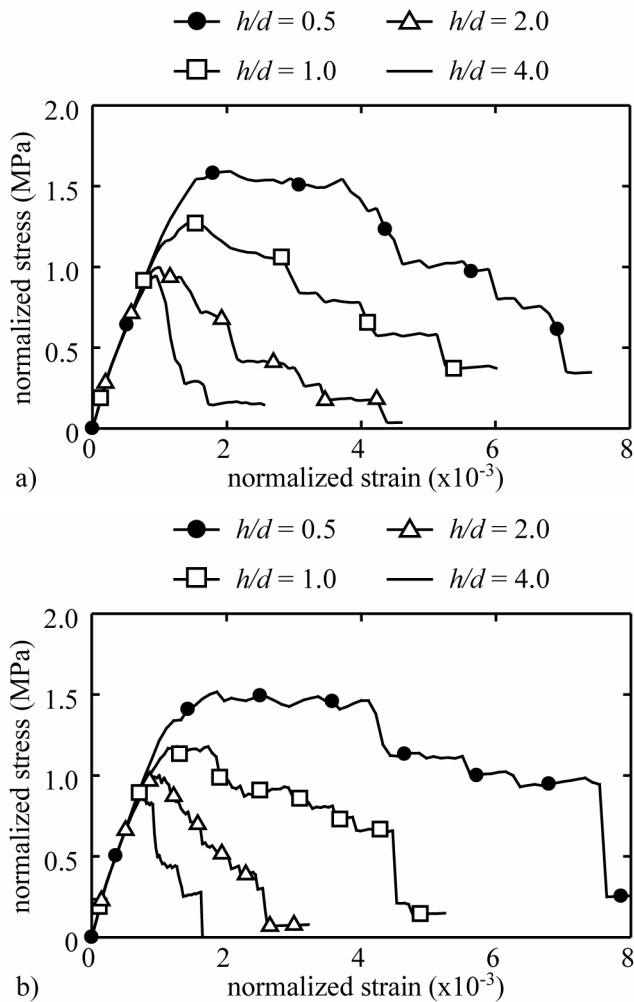


Figure 10. Normalized stress and strain responses for the specimens with high friction: a) effect of slenderness ratio for cylinder specimen; and b) effect of slenderness ratio for prism specimen.

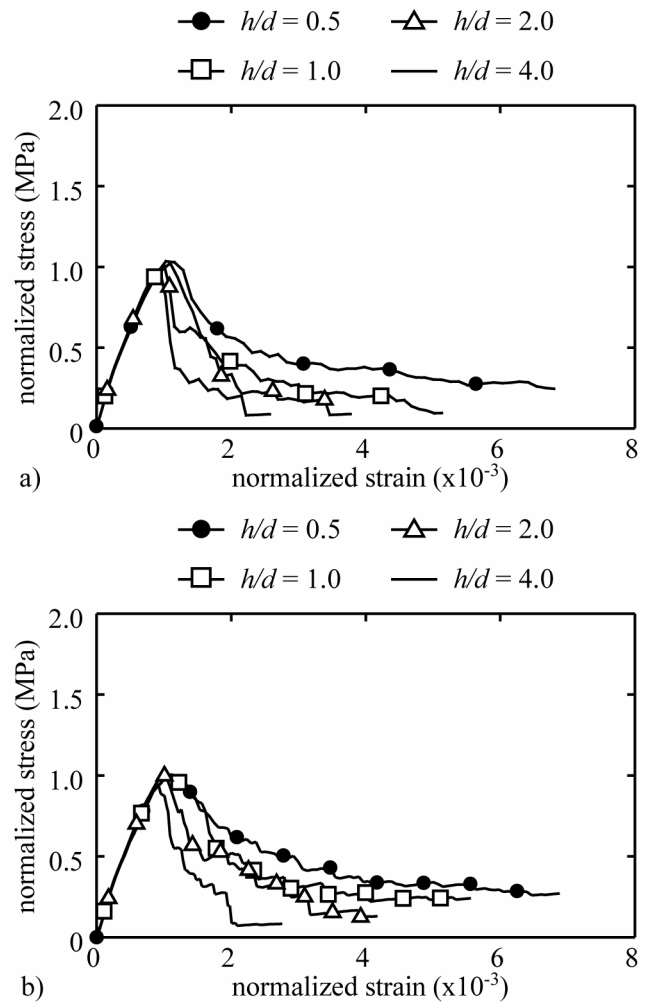


Figure 11. Normalized stress and strain responses for the specimens with low friction: a) effect of slenderness ratio for cylinder specimen; and b) effect of slenderness ratio for prism specimen.

4.2 Simulation results

Figure 10 shows the stress-strain responses obtained from the uniaxial compression test analyses of cylinders and prisms with high friction. The stresses and strains are normalized by the maximum stress (i.e. compressive strength) and the strains at the maximum stress of the specimen with a slenderness ratio $h/d = 2.0$, respectively. The maximum stress increases with decreasing the slenderness ratio. The stress-strain curves are almost the same in the pre-peak regime, but the slope of the descending branch becomes steeper with increasing the slenderness ratio. The normalized stress-strain responses for the cylinders and prisms with low friction are shown in Figure 11. The elimination of friction between the plates and the specimen ends results in an almost constant peak strength, irrespective of the slenderness ratio. The stress-strain responses simulated by the analyses exhibit the same trend observed in the experiments of van Vilet & van Mier (1995).

Figure 12 shows the numerical crack patterns for cylinder specimens with different slenderness ratios and friction conditions. Cracking for the specimens with low friction tends to be aligned in the direction

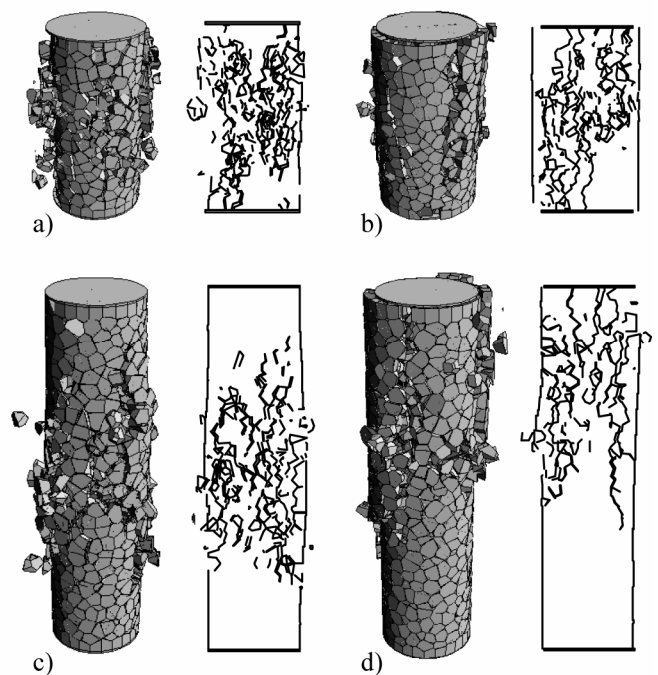


Figure 12. Crack patterns for the cylinder specimens with: a) $h/d = 2.0$ and high friction, b) $h/d = 2.0$ and low friction, c) $h/d = 4.0$ and high friction, and d) $h/d = 4.0$ and low friction

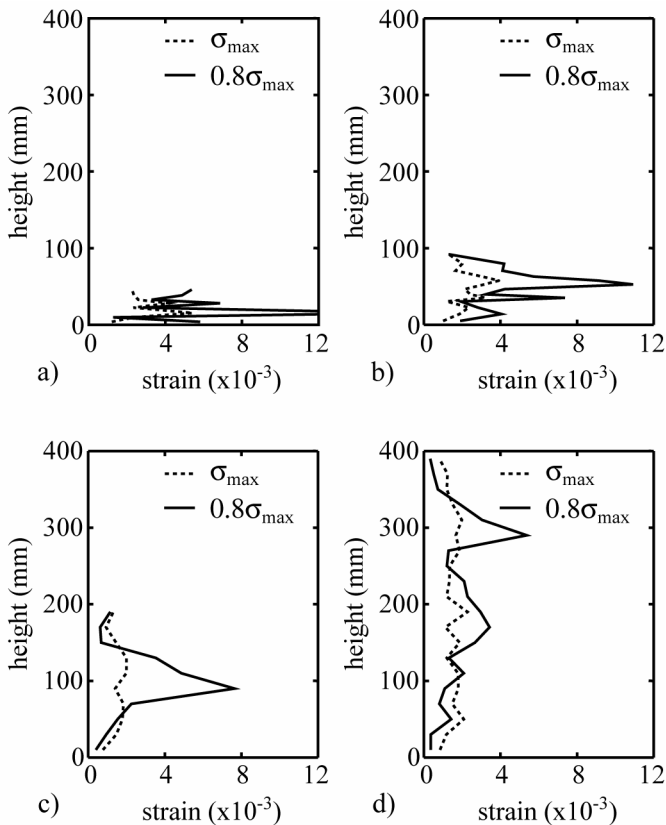


Figure 13. Local strain distributions for: a) a $h/d = 0.5$ specimen, b) a $h/d = 1.0$ specimen, c) a $h/d = 2.0$ specimen, d) a $h/d = 4.0$ specimen.

of compression, while crack development for the specimens with high friction is greatly influenced by the friction between the plates and the specimen ends. As shown in Figure 12c, the confinement effect due to the plate friction does not reach the middle of specimen, therefore the peak stresses for the specimens with larger slenderness ratios are almost the same even if the plate friction is high.

Figure 13 shows the local strain distributions at the peak (σ_{\max}) and after the peak ($0.8\sigma_{\max}$ is 80% of the peak stress) for cylinder specimens with different slenderness ratios in the case of high friction. The local strains along the specimen height are obtained from beam elements placed inside the specimen as shown in Figure 8. Fracture localization can be confirmed by the local increment of strains after the peak stress. For the specimens with smaller slenderness ratios, the local strains after the peak increase throughout the specimen height since the effect of friction between the loading plates and the specimen ends covers the whole range of specimens. Strain localization is, however, clearly observed in the distributions for the specimen with the largest slenderness ratio.

5 CONCLUSIONS

Rigid-body-spring networks are used to investigate the fracture behavior of cement based composites.

The material mesostructure is three-dimensionally modeled using a three component model: mortar matrix, aggregate inclusions, and matrix-inclusion interfaces. Stress-strain responses are well simulated although the material heterogeneity is rather simply treated in order to reduce a computational expense in three-dimensional analyses. This type of modeling is suited to describing ultimate failure mechanisms and post-peak responses, and provides realistic representation of fracture.

The model can simulate the effect of slenderness ratios on the stress-strain responses of cylinder and prism specimens subjected to uniaxial compression. The extreme variation of strength and ductility, which is invoked by friction between loading plates and specimen ends, is well predicted. Crack patterns and local strain distributions obtained from analyses are useful for understanding fracture localization in concrete specimens.

Although the network abilities in three dimensions are well demonstrated, further development is of course needed to obtain more accurate predictions and solve larger problems such as a full model based on an actual mix design.

REFERENCES

- Bazant, Z. P., Tabarra, M. R., Kazemi, T. & Pijiauder-Cabot, G. 1990. Random particle model for fracture of aggregate or fiber composites. *J. Eng. Mech.* 116(8): 1686-1705.
- Bolander, J. E. & Berton, S. 2004. Cohesive zone modeling of fracture in irregular lattices. In V. C. Li et al. (eds.), *Fracture Mechanics of Concrete Structures*: 989-994. Ia-FraMCoS.
- Bolander, J. E. & Saito, S. 1998. Fracture analyses using spring networks with random geometry. *Eng. Fract. Mech.* 61(5-6): 569-591.
- Cusatis, G., Bazant, Z. P. & Cedolin, L. 2003. Confinement-shear lattice model for concrete damage in tension and compression: I. Theory & II. Computation and Validation. *J. Eng. Mech.* 129(12): 1439-1458.
- Kawai, T. 1978. New discrete models and their application to seismic response analysis of structures. *Nuclear Engng. Design* 48: 207-229.
- Liu Y-Q., Hikosaka, H. & Bolander, J. E. 1995. Modeling compressive failure using rigid particle systems. In F. H. Wittmann (ed.), *Fracture Mechanics of Concrete Structures*: 375-382. Freiburg: Aedificatio.
- Otsuka, K. & Katsube, H. 1994. Influences of aggregate size on the behavior of fracture process zone in concrete. *JSCE Concrete Library International* 24: 111-125.
- Schlangen, E. & van Mier, J. G. M. 1992. Experimental and numerical analysis of micromechanics of fracture of cement based composites. *Cem. Conc. Composites* 14(2): 105-118.
- Schlangen, E. 1995. Computational aspects of fracture simulation with lattice models. In F. H. Wittmann (ed.), *Fracture Mechanics of Concrete Structures*: 913-928. Freiburg: Aedificatio.
- van Vilet, M. R. A. & van Mier, J. G. M. 1995. Softening behavior of concrete under uniaxial compression. In F. H. Wittmann (ed.), *Fracture Mechanics of Concrete Structures*: 383-396. Freiburg: Aedificatio.